Annual Report, SCEC Project #080086

Constrained inversions of Geodetic Data from the 2004 Parkfield Earthquake

Kurt Feigl and Clifford Thurber, Principal Investigators
Department of Geology and Geophysics
University of Wisconsin-Madison, Madison, WI 53706
feigl@geology.wisc.edu, thurber@geology.wisc.edu

Introduction

The 2004 M~6 Parkfield earthquake was captured by an extensive array of geophysical instrumentation. Numerous co-seismic slip models of this event have been generated using data from continuously operating Global Positioning System (CGPS) receivers (Figure 1), three-component strong motion instruments, and/or Interferometric Synthetic Aperture Radar (InSAR) (e.g., Custodio et al. (2005); Johanson et al. (2006); Johnson et al. (2006); Liu et al. (2006); Murray and Langbein (2006); Kim and Dreger (2008); Ma et al. (2008); Custodio et al. (2009)). These solutions differ substantially in the details of their slip distributions. the solutions based on geodetic data show the majority of slip occurring 14 to 17 km northwest of the 2004 hypocenter, while those based on strong motion data display the majority of slip occurring at the hypocenter.

Several studies have linked the spatial distribution of aftershocks to the distribution of co-seismic slip and/or stress drop on the fault. This SCEC-funded research project supported the research of graduate student Ninfa Bennington, who explored the use of the distribution of aftershocks as a constraint on a geodetic model of co-seismic fault slip. We present a model for co-seismic slip in the 2004 Parkfield earthquake occurring on the San Andreas Fault (SAF) and Southwest Fracture Zone (SWFZ). The distribution of co-seismic slip was estimated using GPS measurements of co-seismic displacement and applying the 2004 event's aftershock distribution as a constraint. The constraint favors solutions with gradients of co-seismic slip and aftershock density that are anti-parallel in each cell of the modeled fault grid. The slip distribution estimated in our constrained solution more closely resembles distributions derived from strong motion data than do previous solutions based on GPS data. It also yields a better fit to the GPS data.

Data and Method

Co-seismic surface displacements from the 2004 Parkfield earthquake were measured at fourteen stations that recorded signals from the Global Positioning System (GPS) at a 1-Hz sampling rate (Figure 1) (Langbein et al., 2006). The locations of aftershocks following the 2004 earthquake were taken from a catalog of high precision double-difference relocated events from 1984 to 2005 (Thurber et al., 2006). The locations of aftershocks that occurred during the three-month interval following the 2004 Parkfield earthquake were used as a constraint on co-seismic slip.

We adapted the triangular element code of Murray and Langbein (2006) to obtain the co-seismic slip model for the 2004 Parkfield earthquake with the constraint that aftershocks concentrate along the edges of co-seismic slip patches. Initially, the 2004 event's aftershock distribution was applied as a constraint to co-seismic slip using a cross-gradient approach (Gallardo and Meju, 2004). However, it was found that use of the cross-gradient constraint failed to align co-seismic slip patches with aftershock clusters, and instead placed peak co-seismic slip in cells with the highest number of aftershocks.

To work around this issue, we modified the constraint to force the two gradients to be anti-parallel. This approach successfully aligns the edges of co-seismic slip patches with zones of dense aftershocks. To describe the fault geometry, we followed Murray and Langbein (2006). It consists of a single, approximately vertical fault surface below 6 km depth that divides into two fault surfaces above this depth. Of these, the first consists of a main fault surface branching to the northeast to meet the SAF fault trace. The second fault surface continues upwards to meet the Southwest Fracture Zone (SWFZ) trace.

To smooth the slip distribution, we apply a finite-difference approximation of the Laplacian operator separately to each fault surface. This linear problem was solved using the constrained linear least-squares method to minimize the L2-norm of the residual between the calculated and observed data vector. The smoothing and anti-parallel weighting parameters were selected using cross validation as described by Murray and Langbein (2006), where the values that produce the smallest cross validation sum of squares (CVSS) value are considered optimal (Figure 2). We find the optimal values of the smoothing and anti-parallel gradient parameters to be 0.055 and 0.455, respectively.

Results

Figure 3a displays the slip distribution estimated using the anti-parallel constraint. The main fault surface shows the majority of co-seismic slip concentrated between 10 km southeast and 10 km northwest of Carr Hill, with two regions of high slip centered at –5 and +3 km, each with a peak slip value of 0.65 m. These slip patches align with the edges of aftershock clusters. Co-seismic slip on the secondary fault, which intersects the SWFZ, is small with a peak slip of only 0.12 m. The moment for this co-seismic slip model is 1.27×10^{18} N m.

For comparison, the slip distribution of Murray and Langbein (2006) is shown in Figure 3b. This solution uses the same triangular element code and geodetic data, but applies only the smoothing constraint. This model has a co-seismic slip moment of 1.20×10^{18} N m, which is within 6% of the value obtained using the anti-parallel constraint. Co-seismic slip on the main fault surface occurs within a more confined region along strike, between –10 and +2 km southeast of Carr Hill, and consists of only one region of peak slip, centered at –5 km. The secondary fault surface in this model is quite similar in the magnitude and distribution of slip to that of the anti-parallel constrained model, with a peak slip of only 0.16 m. Figure 4 shows the observed and predicted surface displacements for both models. The anti-parallel constrained solution has a variance reduction of 10.2% relative to Murray and Langbein's (2006) solution. Thus, application of the anti-parallel constraint aligns the slip patches along aftershock clusters while improving the fit to the geodetic data. Our slip distribution also more closely resembles those estimated from strong motion, especially the one estimated by Custodio et al. (2009).

Conclusions

We have developed a new model for the distribution of co-seismic slip for the 2004 Parkfield earthquake using co-seismic displacement measured by GPS and applying the aftershock distribution as a constraint. The constraint encourages slip models with gradients of co-seismic slip and aftershock density that are anti-parallel in each cell. This procedure leads to a slip distribution with patches whose edges coincide with areas of high aftershock density. The procedure has the additional effect of improving the predicted fit of the geodetic data relative to the unconstrained case of Murray and Langbein (2006).

The distribution of slip estimated using the anti-parallel constraint agrees well with that estimated from strong motion data where the former is well resolved. The large patch of peak slip northwest of the 2004 hypocenter seen in the anti-parallel constrained solution is in good

agreement in location and amplitude with the geodetic studies and the majority of strong motion studies listed above. The anti-parallel constrained model also shows the continuation of moderate levels of slip southeast of this area, as observed in the majority of strong motion studies examined here. The majority of published geodetic slip models do not contain this continuation of co-seismic slip towards the 2004 hypocenter. One geodetic slip model that does contain this feature is difficult to compare to the anti-parallel constrained slip model because its grid cells are large (~4x4 km) in this region. Southeast of the 2004 hypocenter, the strong motion studies discussed find a patch of peak slip that is absent from the anti-parallel constrained solution determined from GPS data. We find that for inversions derived from GPS data alone, the distribution of these stations prohibits the recovery of a slip patch at or to the southeast of the 2004 hypocenter. Despite this limitation, our anti-parallel constrained solution for co-seismic slip more closely resembles slip models derived from strong motion data than those estimated previously using GPS data.

SCEC Funded Publications

None to date; a manuscript on these results is in preparation.

References

Custodio, S., Liu, P. & Archuleta, R.J., 2005. The 2004 Mw 6.0 Parkfield, California, earthquake; inversion of near-source ground motion using multiple data sets, Geophys.Res.Lett., 32, 4.

Custodio, S. et al., 2009. Constraining earthquake source inversions with GPS data: 2. A two-step approach to combine seismic and geodetic data sets, J.Geophys.Res, 114, B01315.

Gallardo, L. & Meju, M., 2004. Joint two-dimensional DC resistivity and seismic travel time inversion with cross-gradient constraints, J.Geophys.Res, 109, B03311.

Johanson, I.A. et al., 2006. Co-seismic and postseismic slip of the 2004 Parkfield earthquake from space-geodetic data; Special issue on the 2004 Parkfield earthquake and the Parkfield Earthquake Prediction Experiment, Bull. Seism. Soc. Amer., 96, S269-S282.

Johnson, K.M. et al., 2006. Frictional properties on the San Andreas Fault near Parkfield, California, inferred from models of afterslip following the 2004 earthquake; Special issue on the 2004 Parkfield earthquake and the Parkfield Earthquake Prediction Experiment, Bull. Seism. Soc. Amer., 96, S321-S338.

Kim, A. & Dreger, D.S., 2008. Rupture process of the 2004 Parkfield earthquake from near-fault seismic waveform and geodetic records, J.Geophys.Res, 113, B07308.

Langbein, J. et al., 2006. Co-seismic and initial postseismic deformation from the 2004 Parkfield, California, earthquake, observed by Global Positioning System, electronic distance meter, creepmeters, and borehole strainmeters; Special issue on the 2004 Parkfield earthquake and the Parkfield Earthquake Prediction Experiment, Bull. Seism. Soc. Amer., 96, S304-S320.

Liu, P. et al., 2006. Kinematic inversion of the 2004 M 6.0 Parkfield earthquake including an approximation to site effects; Special issue on the 2004 Parkfield earthquake and the Parkfield Earthquake Prediction Experiment, Bull. Seism. Soc. Amer., 96, S143-S158.

Ma, S. et al., 2008. Dynamic modeling of the 2004 Mw 6.0 Parkfield, California, earthquake, J. Geophys.Res, 113, B02301.

Murray, J. & Langbein, J., 2006. Slip on the San Andreas Fault at Parkfield, California, over two earthquake cycles, and the implications for seismic hazard; Special issue on the 2004 Parkfield earthquake and the Parkfield Earthquake Prediction Experiment, Bull. Seism. Soc. Amer., 96, S283-S303.

Thurber, C., et al., 2006. Three-dimensional compressional wavespeed model, earthquake relocations, and focal mechanisms for the Parkfield, California, region, Bull. Seism. Soc. Am., 96, S38-S49.

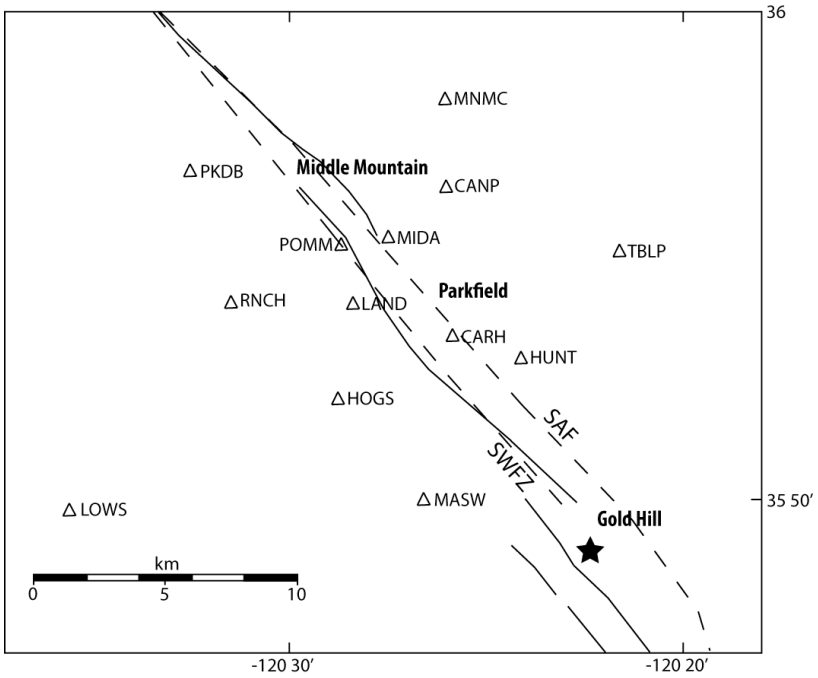

Figure 1. (a) Locations of continuously operating GPS receivers for the Parkfield region (shown as white triangles). Dashed black lines represent the main and secondary fault surfaces intersection with the SAF and SWFZ surface traces respectively. Solid black lines represent surface traces for the SAF and its subsidiary faults. Epicenter of 2004 Parkfield earthquake indicated as solid black star. Figure adapted from Murray and Langbein (2006).

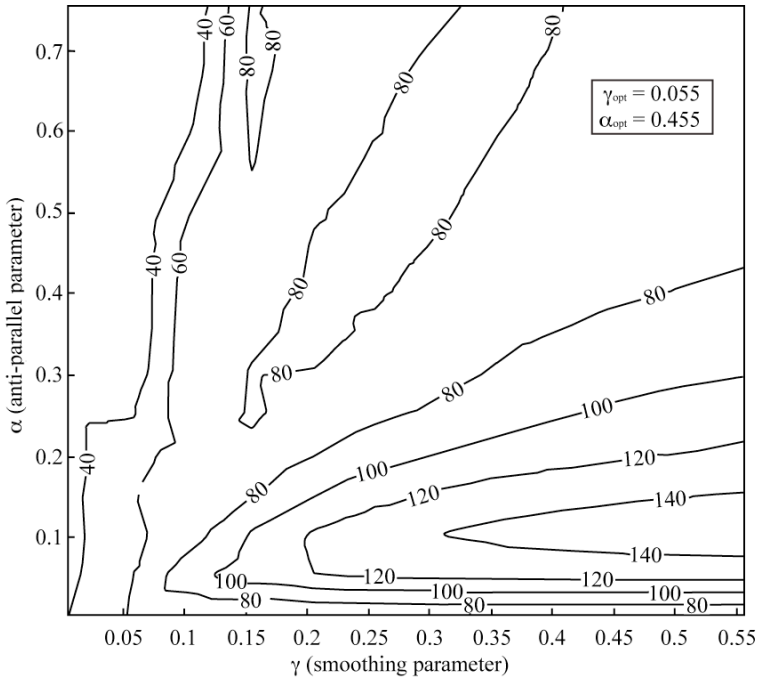

Figure 2. Contours of misfit showing the trade-off between the anti-parallel parameter versus smoothing parameter for the anti-parallel constrained solution. Contour lines represent CVSS for particular parameter pairs.

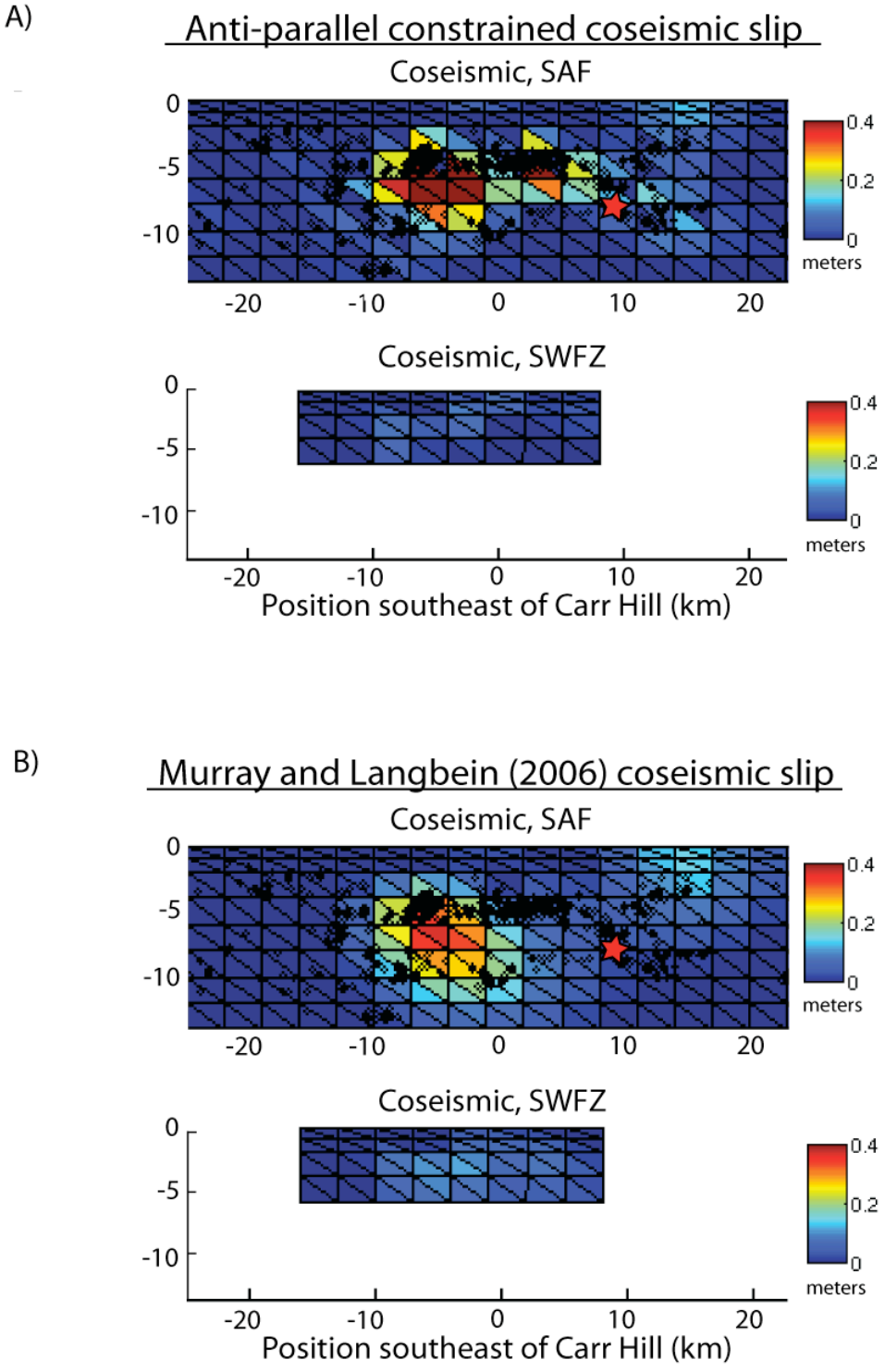

Figure 3. Distribution of co-seismic slip for the 2004 Parkfield earthquake, as estimated with the anti-parallel constraint (a, this study) and without any information regarding the aftershock locations (b, Murray and Langbein, 2006). Both solutions use the same fault geometry using triangular cells. For both (a) and (b), the upper and lower panels show magnitude of co-seismic slip on main and secondary fault surfaces with magnitude of slip represented on color bar. Locations are shown with respect to GPS station CARH. The location of 2004 hypocenter is indicated by red star.